

Article

Using Hyperspectral Imaging and Principal Component Analysis to Detect and Monitor Water Stress in Ornamental Plants

Van Patiluna ¹, James Owen, Jr. ², Joe Mari Maja ^{1,*}, Jyoti Neupane ³, Jan Behmann ⁴, David Bohnenkamp ⁴, Irene Borra-Serrano ⁵, José M. Peña ⁵, James Robbins ⁶ and Ana de Castro ⁷

¹ Center of Applied Artificial Intelligence for Sustainable Agriculture, 1890 Research and Extension, Public Service and Agriculture, South Carolina State University, 300 College Avenue, Orangeburg, SC 29117, USA; vpatilun@scsu.edu

² Application Technology Research Unit, United States Department of Agriculture, Agricultural Research Service, 1680 Madison Ave., Wooster, OH 44691, USA; jim.owen@usda.gov

³ Department of Crop and Soil Sciences, Miller Plant Sciences, 120 Carlton Street, Athens, GA 30602, USA; jn78616@uga.edu

⁴ Institute for Crop Science and Resource Conservation, Plant Diseases and Plant Protection, University of Bonn, 53115 Bonn, Germany; jan.behmann@gmail.com (J.B.); david.bohenenkamp@gmx.net (D.B.)

⁵ Institute of Agricultural Sciences (ICA), Spanish National Research Council (CSIC), 28006 Madrid, Spain; irene.borra@ica.csic.es (I.B.-S.); jmpena@ica.csic.es (J.M.P.)

⁶ Ornamental Hort Solutions, 300 N Pine St, Little Rock, AR 72205, USA; jrobbins4930@gmail.com

⁷ Environment and Agronomy Department, National Agricultural and Food Research and Technology Institute (INIA), Spanish National Research Council (CSIC), 28040 Madrid, Spain; ana.decastro@csic.es

* Correspondence: jmaja@scsu.edu



Academic Editor: Ruyin Cao

Received: 20 November 2024

Revised: 3 January 2025

Accepted: 12 January 2025

Published: 15 January 2025

Citation: Patiluna, V.; Owen, J., Jr.; Maja, J.M.; Neupane, J.; Behmann, J.; Bohnenkamp, D.; Borra-Serrano, I.; Peña, J.M.; Robbins, J.; de Castro, A. Using Hyperspectral Imaging and Principal Component Analysis to Detect and Monitor Water Stress in Ornamental Plants. *Remote Sens.* **2025**, *17*, 285. <https://doi.org/10.3390/rs17020285>

Copyright: © 2025 by the authors.

Licensee MDPI, Basel, Switzerland.

This article is an open access article distributed under the terms and conditions of the Creative Commons Attribution (CC BY) license (<https://creativecommons.org/licenses/by/4.0/>).

Abstract: Water stress is a critical factor affecting the health and productivity of ornamental plants, yet early detection remains challenging. This study aims to investigate the spectral responses of four ornamental plant taxa—*Rosa* hybrid (rose), *Itea virginica* (itea), *Spiraea nipponica* (spirea), and *Weigela florida* (weigela)—under varying levels of water stress using hyperspectral imaging and principal component analysis (PCA). Hyperspectral data were collected across multiple wavelengths and PCA was applied to identify key spectral bands associated with different stress levels. The analyses revealed that the first two principal components captured a majority of variance in the data, with specific wavelengths around 680 nm, 760 nm, and 810 nm playing a significant role in distinguishing between the stress levels. Score plots demonstrated clear separation between different stress treatments, indicating that spectral signatures evolve distinctly over time as water stress progresses. Influence plots identified observations with disproportionate impacts on the PCA model, ensuring the robustness of the analysis. Findings suggest that hyperspectral imaging, combined with PCA, is a powerful tool for early detection and monitoring of water stress in ornamental plants, providing a basis for improved water management practices in horticulture.

Keywords: water stress; ornamental plants; hyperspectral imaging; principal component analysis; precision agriculture

1. Introduction

The nursery industry significantly contributes to the United States economy, providing substantial economic value and employment opportunities. Behe et al. (2008) reported that nursery production contributed USD 18.1 billion to the US economy in 2002 and created nearly 2,000,000 jobs [1]. This economic impact underscores the importance of the nursery sector in supporting livelihoods and driving economic growth. Additionally,

Hall et al. (2020) [2] highlighted that nursery and greenhouse production firms accounted for a substantial number of jobs and contributed significantly to the GDP, emphasizing the industry's economic significance. In the context of nursery production, water stress in ornamental plants poses a critical challenge. Toscano et al. (2019) [3] discussed the responses of Mediterranean ornamental plants to drought stress, which include alterations in root-to-shoot ratio, growth reduction, changes in leaf anatomy, and reductions in leaf size and total leaf area. The biophysical alterations collectively minimize water loss to ensure optimal photosynthesis and subsequent carbon assimilation. Understanding these responses is crucial for nursery operators to implement effective water management strategies and mitigate the impact of water stress, plant health and growth. Majsztrik et al. (2017) [4] highlighted the reliance of specialty crop producers, including nursery operations, on high-quality fresh water from surface and groundwater sources for containerized production. Water availability and quality are essential considerations in nursery production as inadequate water supply or poor water management practices can exacerbate water stress in ornamental plants. Álvarez and Sánchez-Blanco (2013) [5] emphasized the importance of accurately scheduling irrigation to match water loss through evapotranspiration from the crop canopy and soil, underscoring the need for precise irrigation management in container ornamental nurseries with little water storage within the substrate to address water stress effectively. Efforts to address water stress in ornamental plants in nursery production involve various strategies including adopting advanced technologies and practices. Cameron et al. [6] controlled water stress to manage shoot growth in container-grown Rhododendron cv. Hoppy, demonstrating that regulated water stress can reduce excessive growth and subsequent need to prune, leading to more compact and marketable plants. Similarly, Scagel et al. [7] explored irrigation frequency and nutrient uptake in container-grown Rhododendron species, demonstrating that careful water management can minimize stress while supporting plant growth. These studies underscore the potential of water management techniques to optimize water use and plant health in nurseries through both stress-based and technology-driven solutions.

The nursery industry significantly contributes to the U.S. economy, providing substantial economic value and employment opportunities. However, water stress in ornamental plants poses a significant challenge for nursery operators, necessitating the adoption of effective water management strategies and innovative solutions to mitigate the impact of drought stress on plant health and productivity [8]. By integrating advanced technologies, precise irrigation practices, and biological interventions, nurseries can enhance water use efficiency, optimize plant responses to water stress, and sustainably manage water resources in ornamental plant production.

Hyperspectral cameras have gained significant attention in agriculture due to their ability to provide detailed spectral information beyond the capabilities of traditional RGB cameras [9]. These advanced imaging devices capture a wide range of wavelengths across the electromagnetic spectrum, enabling the detection of subtle changes in plant health and stress levels [8]. They have been widely applied in plant phenotyping, disease detection, and monitoring stress factors such as water stress [10,11]. By analyzing the reflected spectral signatures of plants, hyperspectral imaging offers valuable insights into the early onset of diseases and stress factors, facilitating timely interventions to mitigate potential crop losses [12,13]. Furthermore, hyperspectral imaging has been instrumental in exploring natural plant diversity to improve tolerance to stressors like excess salt, contributing to sustainable agricultural practices [14].

Hyperspectral cameras have shown great promise in the specific context of discriminating water stress levels in crops. By analyzing hyperspectral imagery and utilizing machine learning algorithms, researchers have been able to estimate water stress in mono-

cultured crops (i.e., potato) with a high degree of accuracy [13]. The spectral information captured by hyperspectral cameras allows for the development of spectral indices that can indicate the water status of plants, enabling farmers to make informed decisions regarding irrigation and water management strategies [15]. This technology has the potential to revolutionize how water stress is monitored in agricultural settings leading to more efficient water usage and improved crop yields. Moreover, hyperspectral imaging has been used to discriminate between different types of stress factors affecting plants, including abiotic and biotic stresses. By analyzing hyperspectral data, researchers have been able to differentiate between drought stress caused by environmental factors and stress induced by pests or diseases [16]. This capability is crucial for farmers to accurately diagnose the underlying causes of stress in their crops and implement targeted interventions to address specific stressors effectively. Furthermore, the combination of hyperspectral imaging with advanced technologies such as artificial neural networks and deep learning has enhanced the detection and identification of plant diseases. By training algorithms on hyperspectral images, researchers have developed models capable of identifying specific pathogens affecting plants, such as viruses and pests [17]. This approach not only aids in early disease detection but also enables researchers to track the spread of diseases and assess their impact on crop health. In the realm of precision agriculture, hyperspectral cameras have proven to be valuable tools for monitoring crop health and optimizing agricultural practices. By providing detailed information about plant physiological processes, hyperspectral imaging can assist farmers in making data-driven decisions to enhance crop productivity and sustainability [18]. Using hyperspectral data to assess biomass, nitrogen content, and other key indicators of plant health enables farmers to implement targeted interventions and maximize yields while minimizing resource inputs. Virnodkar et al. emphasized the critical role of machine learning in analyzing hyperspectral data for various crops, underscoring its potential to enhance water stress determination [19]. The ability of these algorithms to process large datasets and identify subtle variations in spectral signatures is crucial for timely intervention in agricultural practices. Physiological indicators of water stress have also been a focal point in recent studies. Wong et al. utilized hyperspectral reflectance to phenotype the physiological drought response in common and tepary beans, measuring parameters such as stomatal conductance and leaf water potential (LWP) [20]. These indicators are sensitive to changes in plant water content and stress, providing a direct link between hyperspectral data and plant health. Furthermore, Park et al. explored the relationship between canopy temperature and water stress, using UAV-borne thermal sensing alongside hyperspectral imaging to monitor plant water status effectively [21]. This multi-faceted approach highlights the importance of integrating different sensing modalities to enhance the understanding of plant responses to water availability. Technological innovations in hyperspectral imaging systems have also contributed to advancements in water stress detection. The development of UAV-borne hyperspectral systems has made high-resolution data collection more accessible and efficient. Liu et al. designed a UAV-based hyperspectral imaging system specifically for water quality monitoring, showcasing the versatility of these technologies in agricultural applications [22]. Additionally, the continuous improvement of hyperspectral sensors, which capture a wide range of spectral bands, allows for more precise assessments of plant health and stress levels [23]. This capability is essential for precision agriculture, where timely and accurate data can significantly impact crop management decisions. Susić et al. demonstrated the ability of hyperspectral imaging to differentiate abiotic from biotic stress in tomato plants, emphasizing the role of spectral analysis in diagnosing and addressing complex stress scenarios [16]. Similarly, Zeng et al. presented an improved hyperspectral index for monitoring water stress in real-time field conditions, highlighting the potential for integrating this technology into large-scale agricul-

tural practices [24]. These recent studies underscore the growing adoption of hyperspectral imaging in stress detection and its applicability to dynamic agricultural environments. Hyperspectral cameras have revolutionized the field of agriculture by offering a non-invasive and comprehensive way to monitor plant health, detect diseases, and assess stress factors such as water stress. The detailed spectral information provided by hyperspectral imaging allows for precise analysis of plant conditions, enabling farmers and researchers to make informed decisions to optimize crop production and sustainability. As technology advances, hyperspectral imaging is poised to play an increasingly vital role in shaping the future of agriculture by providing valuable insights into plant health and stress factors.

The objective of this work was to investigate and quantify the spectral responses of four ornamental plant taxa—*Rosa* hybrid (rose), *Itea virginica* (itea), *Spiraea nipponica* (spirea) and *Weigela florida* (weigela)—under varying levels of water stress. Utilizing hyperspectral imaging combined with principal component analysis (PCA), the study aims to identify key spectral bands associated with physiological changes induced by water deprivation. By analyzing how these spectral signatures evolve over time, the research seeks to develop reliable indicators of crop water stress spatially across taxa that can be used for early detection and monitoring of ornamental plant species, ultimately contributing to improved water management practices. These taxa were selected to represent a diverse range of morphological characteristics and drought tolerance levels, providing a spectrum of responses to water stress. *Rosa hybrid*, a widely cultivated ornamental species, was included for its economic importance and high sensitivity to drought conditions. *Itea virginica* and *Spiraea nipponica*, with moderate drought tolerance, were chosen as examples of shrubs that can endure varying levels of stress. *Weigela florida*, known for its robust morphology and higher drought tolerance, was included to assess the sensitivity of hyperspectral imaging in detecting subtle stress responses. This selection ensures that the findings are broadly applicable to ornamental plants with varying physiologies and drought adaptations.

2. Materials and Methods

The experiment was conducted at the Hampton Roads Agricultural Research and Extension Center, Virginia Beach, VA, USA. The nursery pad used for this experiment was prepared to accommodate a grid layout for plant placement and sensor analysis. Figure 1 shows the four ornamental plant taxa used in the experiment to evaluate the effects of water stress: rose, itea, spirea, and weigela. These taxa were chosen to represent a range of morphological traits and drought tolerance levels, ensuring diverse responses to water stress for analysis. Rose, a widely cultivated and economically important species, is highly sensitive to drought. Itea and spirea were selected for their moderate drought tolerance, while weigela—known for its robust morphology—was included to evaluate hyperspectral imaging's ability to detect subtle stress responses.

2.1. Morphological and Drought Response Characteristics of Four Ornamental Plant Taxa

Table 1 provides detailed descriptions and measurements for four ornamental plant taxa used in the study: *Weigela florida* ("Czechmark Trilogy™"), *Itea virginica* ("Scentlandia®"), *Spiraea nipponica* ("Wedding Cake®"), and rose hybrid ("Julia Child™"). Each taxon was characterized by specific morphological traits, including average height, width, and substrate depth as well as qualitative descriptions of leaf structure, color, and overall plant form.



Figure 1. Images of the four ornamental plant taxa used in the study.

Table 1. Morphological traits and drought response characteristics of four ornamental plant taxa used in the study.

Genus Species Cultivar	Czechmark Trilogy™ Weigela Florida "VUKOZGemini"	Scentlandia® Itea Virginica "SMNIVDFC"	Wedding Cake® Spiraea Nipponica "SMNSNFD"	Julia Child™ Rose; Rosa Hybrid "Wekvossutono"
USPP/Patent	USPP 28,969, Can PBRAF	USPPAF, Can PBRAF	USPP 28,096, Can PBRAF	Plant Patent #18,473
Average Height (n = 10)	30.9 cm ± 2.8 SD	67.8 cm ± 4.3 SD	27.0 cm ± 2.7 SD	38.0 cm ± 4.7 SD
Average Widest Width (n = 10)	55.1 cm ± 4.1 SD	75.8 cm ± 8.4 SD	49.9 cm ± 3.8 SD	63.7 cm ± 5.7 SD
Average Perpendicular Width (n = 10)	46.2 cm ± 4.2 SD	63.9 cm ± 7.9 SD	43.1 cm ± 4.1 SD	55.9 cm ± 4.9 SD
Average Substrate Depth (n = 5)	3.8 cm ± 0.67 SD	2.8 cm ± 0.76 SD	3.4 cm ± 0.75 SD	3.0 cm ± 0.82 SD
Description	Round flowering shrub with coarse texture. Notable small pink/white flowers along stems/leaves. Leaves ranging in size from small and narrow for vigorous, newer growth to larger, broader leaves on older growth or sucker like shoots. Light- to medium-green leaves were cupping and had curling margins which was more pronounced in older, larger leaves. Moderately resistant to drought showing increased leaf curling.	Upright, vase-shaped, flowering shrub with medium- to light-green foliage. Newest foliage/shoots had rust-red-like appearance in color, but more were light-green. Leaves were held at less horizontal to 45 degree angle of stem. Leaf angle/droop becomes more pronounced as leaf stem/tissue loses turgor.	Flowering ground cover/shrub with fine texture and spreading habit. Blue/green fine foliage with linear-narrow leaves in horizontal orientation. Newer growth/stems directly upright. Poor drought resistance with leaves losing turgor rapidly.	Rose is a round flowering shrub that has a medium texture and dark- to medium-green foliage that is glossy. The newest growth is reddish in color. Plants were in all stages of flowering. Yellow flowers. Leaves are primarily oriented horizontally.

Following the collection of hyperspectral images, one plant was randomly selected from each water stress level for each plant taxa and photographed as shown in Figures 2–5.

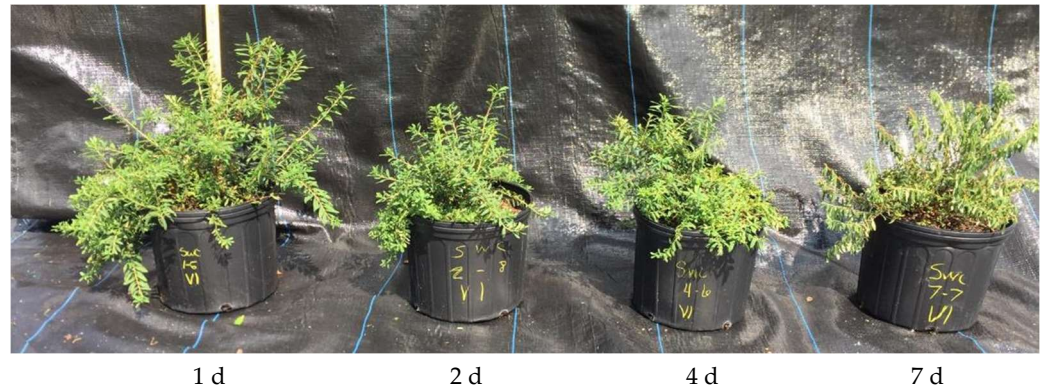


Figure 2. Photographs of one plant randomly selected from each water stress level for spirea following the collection of hyperspectral images. Numbers below each plant indicate the number of days water was withheld.



Figure 3. Photographs of one plant randomly selected from each water stress level for rose following the collection of hyperspectral images.



Figure 4. Photographs of one plant randomly selected from each water stress level for itea following the collection of hyperspectral images.

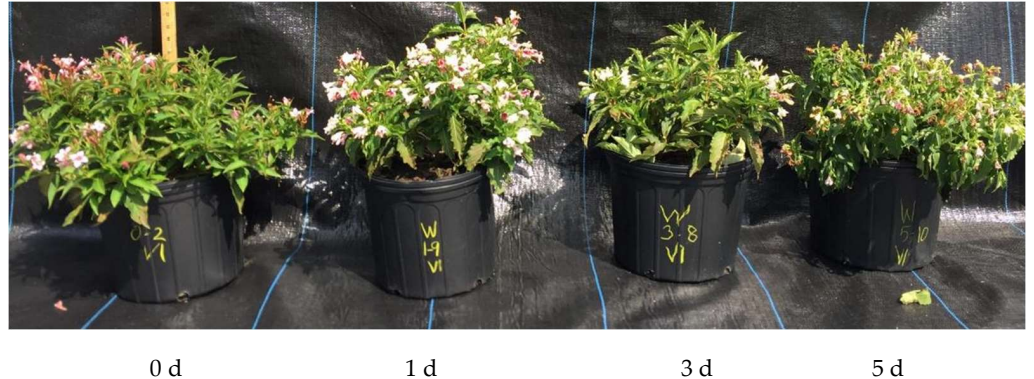


Figure 5. Photographs of one plant randomly selected from each water stress level for weigela following the collection of hyperspectral images.

Weigela is noted for its round shape, coarse texture, and moderate drought resistance, displaying leaf curling under stress. Itea features an upright, vase-like form with medium-to light-green foliage and high drought resistance, showing leaf droop under severe water stress. Spirea presents as a fine-textured, spreading ground cover with poor drought resistance, characterized by blue-green foliage. Rose hybrid is a medium-textured, round shrub with dark-green, glossy leaves and ongoing flowering, showing resilience across different growth stages. These observations provide critical insights into the physical responses of these taxa under varying environmental conditions.

2.2. Plant Arrangement and Treatment

Eleven-liter (#3, C1200, Nursery Supplies, Chambersburg, PA, USA) containers filled with a pine bark substrate amended with dolomite and controlled release fertilizer were used to grow the four taxa under overhead irrigation. Plants were pruned to maintain a healthy and uniform canopy until experiment initiation. All taxa were subjected to four distinct levels of water stress, with five plants ($n = 5$) allocated to each stress level. To maintain experimental rigor, treated plants were interspersed among 50 non-water stressed control plants of the same taxon. Plants were arranged in a 7×10 grid pattern to ensure even spacing which facilitated uniform conditions for the experiment as shown in Figure 6. Taxa were grouped into four distinct areas on the nursery pad, with each area corresponding to a specific taxon. Area 1 was designated for weigela, Area 2 for spirea, Area 3 for itea, and Area 4 for rose, as indicated by the numbers in the image.



Figure 6. The experimental layout on the nursery pad for rose (4), itea (3), spirea (2), and weigela (1). Plants located on the edge were used for training and center sections for validation in a 7×10 grid pattern.

2.3. Training and Validation Areas

The sides of each group, as marked in the image (Figure 7), were designated as training areas. Here, plants were used to calibrate the hyperspectral imaging sensors and to develop predictive models. These training areas are crucial for establishing baseline spectral data and ensuring the accuracy of the subsequent analysis.



Figure 7. The experimental layout shows the arrangement of rose, itea, spirea, and weigela plants in 7×10 grids, with designated validation plants and stress levels indicated for each taxon.

The center of each group served as the validation area. Plants in these sections were used to test the predictive models developed from the training data to assess the models' accuracy and generalizability under real-world conditions. This approach helped minimize potential external variables, ensuring that the hyperspectral imaging results were both reliable and reproducible.

Water stress was induced by removing the selected plants from their regular irrigation schedule and withholding water for varying durations of up to 7 days. The water stress levels were defined as follows: Level 0 for well-watered plants, Level 1 for 1 day without water, Level 2 for 2 days without water, Level 3 for 3 days without water, Level 4 for 4 days without water, Level 5 for 5 days without water, and Level 7 for 7 days without water. The non-water stressed plants continued to receive regular irrigation throughout the experiment.

2.4. Preparation and Handling of Plants

Plants were carefully removed from their respective growing areas and saturated to effective container capacity as outlined in Fields et al. [25]. This saturation process was achieved through hand watering using a wand and breaker. Each plant received three rounds of watering, with each round lasting a minimum of 3 s. To ensure thorough saturation, a 1 min interval was maintained between each watering event, allowing the substrate to fully absorb water between rounds.

Following this saturation procedure, plants were allowed to drain for a standardized period of 30 min to remove excess water while retaining sufficient moisture within the container capacity. After draining, each plant was weighed individually using a Defender 3000 scale (model #D30BR, Ohaus Corp, Parsippany, NJ, USA) to obtain accurate weight measurements corresponding to their fully saturated state.

On August 21, all plants were initially positioned on a bench in a glass covered greenhouse. To protect them from any precipitation and ensure consistent drying conditions, plants were then transferred to gravel ground cover adjacent to the greenhouse on August 22, where they remained until August 27. This gravel-covered area minimized

unintended water input while allowing for a controlled drying environment. Plants designated for drying treatments (i.e., those not receiving any water) stayed on the gravel ground cover to ensure consistency in water stress application. On August 28, plants were weighed again before being assigned as training plants or randomly allocated as validation plants within the experimental setup. This preparation ensured a consistent and controlled baseline for both the training and validation phases of the study.

2.5. Hyperspectral Imaging

Five #3 flowering shrubs at each of the four water stress levels ($n = 5$) and five non-water-stressed plants were grouped by treatment. These plants were placed adjacent to the experimental block and used to train and calibrate the hyperspectral imaging sensors.

The hyperspectral camera (Rikola, Senop, Helsinki, FI, USA) (Figure 8a) was used to collect hyperspectral data. The camera is a snapshot with spectral region from 503–898 nm. The selected configuration measured 55 bands equally distributed in 7 nm steps with 8–12 nm Full Width at Half Maximum (FWHM). It has a 1010×1010 pixel spatial resolution and 1.5 s measurement time. Calibration was performed using a 50% grey reference panel (SphereOptics GmbH, Herrsching, Germany) on each flight. The reference panel images were captured immediately before and after the imaging of the plants to ensure consistent normalization under varying lighting conditions. The hyperspectral camera was mounted to an unmanned aerial system (Matrice 600 Pro, DJI, Shenzhen, China) (Figure 8b) with a 3-axis gimbal (Ronin, DJI, Shenzhen, China).



Figure 8. (a) Hyperspectral camera used for data collection, and (b) camera mounted on the Matrice 600 Pro drone for aerial imaging.

For each plant, hyperspectral data were collected from three distinct points in the canopy. The average of these three points was calculated to represent the spectral signature of each individual plant. This approach helped to account for any intra-plant variability and ensured a more reliable representation of the plant's water stress level. The raw hyperspectral data were corrected for sensor-specific distortions and noise using the manufacturer's software (Senop HSI-2 v.2020.01.03.1), which included radiometric and geometric corrections. Radiometric correction accounted for the camera's sensitivity across different wavelengths, and geometric correction ensured proper alignment of spectral bands. Reflectance data were then normalized using the grey reference to generate consistent spectral signatures. Outlier pixels or anomalous data were identified and excluded during preprocessing to ensure the quality and reliability of the spectral data.

2.6. Data Analysis

Data analysis in this study involved hyperspectral imaging data collected from four ornamental plant taxa—rose, itea, spirea, and weigela—subjected to varying levels of water stress. For each taxon, spectral data were collected across multiple wavelengths, capturing the reflectance characteristics of the plants under different stress levels. Data points for this study were selected through a systematic approach aimed at capturing representative measurements across varying water stress levels and ensuring consistency within each taxon. For each plant, spectral data were collected from three distinct points to account for intra-plant variability and provide a comprehensive representation of each plant's physiological state. These three data points were averaged to produce a single, consolidated spectral signature per plant, minimizing potential variability and noise due to localized differences within the canopy.

PCA was employed to analyze this high-dimensional data utilizing the singular value decomposition (SVD) algorithm. SVD was chosen for its robustness and ability to handle large datasets efficiently. The analysis aimed to reduce the dimensionality of the data while retaining the most significant variance, enabling the identification of key spectral bands associated with water stress.

The PCA model was validated using cross-validation, specifically a full cross-validation method with 20 segments. This approach allowed for a thorough assessment of the model's performance and ensured that the results were reliable and generalizable. The analysis considered seven components, with the model suggesting four as the optimal number of components. This optimal number was determined to be four based on the explained variance and the ability to distinguish between different levels of water stress.

3. Results

3.1. Rose

The PCA for rose cultivar aims to explore the spectral variations and responses to different water stress levels. The stress levels are represented by the number of days without water (D0, D2, D4, and D7, corresponding to 0, 2, 4, and 7 days, respectively). The analysis focuses on identifying the key spectral bands contributing to the differentiation between these stress levels and understanding how the rose plants' spectral signatures evolve over time under water stress conditions.

3.1.1. Explained Variance

The explained variance plot (Figure 9) for rose illustrates the percentage of data variance captured by each principal component (PC) for both the calibration and validation datasets. For the calibration dataset, PC-1 explains 77% of the variance, with cumulative explained variance reaching 86% by PC-2 and over 91% by PC-3. This trend indicates that the first few components capture the majority of the variability in the data, making them essential for understanding spectral responses.

In the validation dataset, the cumulative variance is somewhat lower, with PC-1 capturing 67% of the variance and PC-2 bringing the total to approximately 72%. The cumulative variance reaches around 76% by PC-3. Although the validation set variance is lower than that of the calibration, the first few components still represent a substantial portion of the variance, affirming the model's consistency. The steep drop in explained variance after PC-2 indicates that the remaining principal components contribute very little additional explanatory power. This suggests that most of the meaningful information in data are concentrated in the first two components, and the other components primarily capture noise or very minor variations. This allows for a significant reduction in data

dimensionality without losing critical information making the analysis more efficient and easier to interpret.

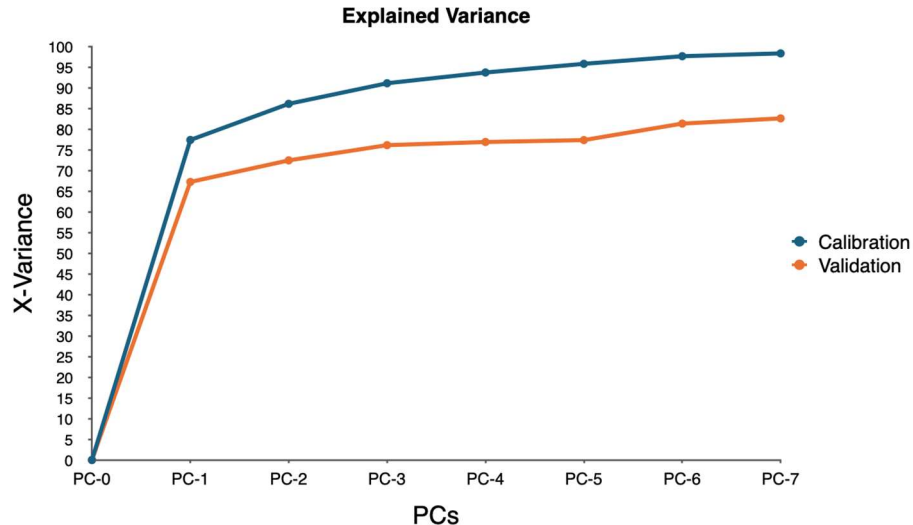


Figure 9. Explained variance plot for rose, showing cumulative variance captured by each principal component in calibration and validation datasets, with the first three components capturing the majority of data variability.

The dominance of PC-1 in explaining the variance underscores its importance in distinguishing between the different water stress levels in the rose plants. The contribution of PC-2, while smaller, is still crucial, as it helps capture additional nuances in the data that could be related to variations in the plant canopy, physiology, or architecture that occur when a crop undergoes water stress and cascading biotic stressors due to stomatal closure and reduced gas exchange, leaf temperature rise, and inability to quench free damaging radicals. This explained variance pattern suggests that a limited number of components, especially the first three, are sufficient to capture the primary variability in rose's spectral data. This consistency between calibration and validation sets implies that the model is robust in identifying key spectral characteristics related to water stress in rose.

3.1.2. Scores Plot

The scores plot (Figure 10) for rose illustrates the distribution of data points across the first two principal components, PC-1 (77% variance explained) and PC-2 (9% variance explained). Each point represents a specific day under varying levels of water stress (D0, D2, D4, and D7). The separation of points along PC-1 and PC-2 highlights distinct clustering and dispersion patterns that reveal rose's physiological response to water stress over time.

The substantial variance explained by PC-1 (77%) indicates that this component captures the primary physiological response of rose to water stress. Data points for D0, representing the control (unstressed) condition, generally appear on the left side of the plot, while points for D4 and D7, indicating more prolonged stress, tend to progressively shift toward the right, illustrating data sensitivity. This separation along PC-1 suggests that as water stress intensifies, rose's spectral response shifts, likely due to changes in water content, leaf angle and size, or physiological response to reduced gas exchange that is exacerbated over time.

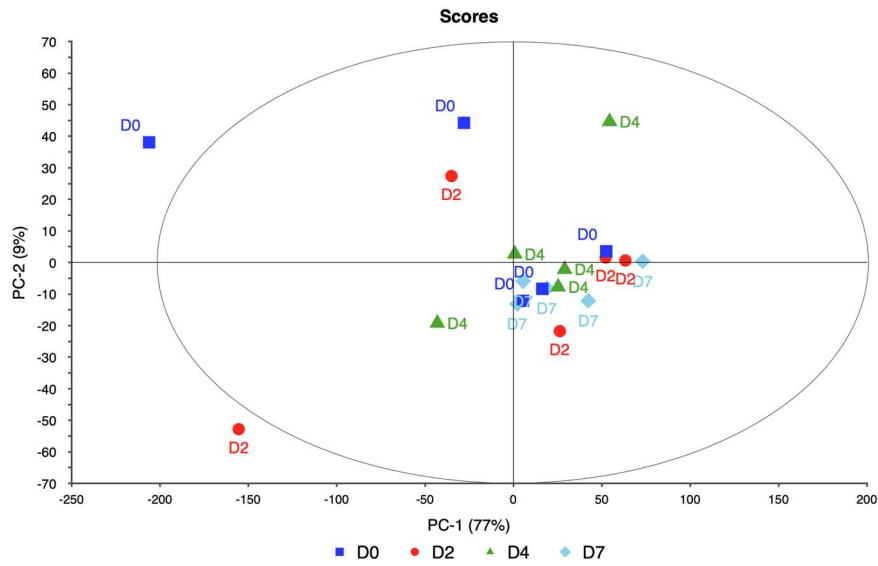


Figure 10. Scores plot for rose showing the distribution of spectral responses across water stress levels, with PC-1 capturing primary stress responses and PC-2 highlighting secondary variations.

PC-2, although explaining a smaller portion of the variance (9%), captures additional, secondary variation in spectral response of rose canopy to water stress. The spread along PC-2 is more variable across all stress levels, indicating that this component reflects subtle physiological changes or individual variability in response to stress. Points from D2 show a wider range along PC-2, suggesting that the early stages of stress induce inconsistent spectral responses among different plants, potentially due to the subtleness of changes, plant's initial adaptation processes or slight differences in individual tolerance levels.

Distinct clustering can be observed among points from D0 and D7, indicating a relatively uniform response in the unstressed and most stressed states. In contrast, data points from D2 and D4 exhibit a more dispersed pattern, especially along PC-2, reflecting the intermediate responses of rose as it adjusts to increasing water stress. This dispersion in the middle stress levels may highlight transitional physiological states, where some plants begin to show signs of significant stress while others are less affected, potentially due to minor variances in root architecture and ability to acquire plant available water, preexisting drought tolerance that occurred during the production of plants, allowing the plant to better regulate physiology according to induced stress. Future studies could use other methods that rapidly create plant water stress; however, this would still lead to confounding abiotic stressors.

The scores plot demonstrates that PC-1 effectively captures the main response of rose to water stress, with a clear separation between early, intermediate, and advanced stress levels. Meanwhile, PC-2 reveals additional complexity in the response, particularly at intermediate stages of stress, which could indicate the onset of adaptive or defensive physiological mechanisms. Together, these components offer a comprehensive view of response trajectory of rose under drought conditions, supporting the use of hyperspectral imaging to monitor early and progressive signs of water stress in this ornamental species.

3.1.3. Correlation Loadings

The correlation loadings plot (Figure 11) for rose illustrates the relationship between specific spectral bands and the first two principal components (PC-1 and PC-2), which explain 77% and 9% of the total variance, respectively. Each point on the plot represents a wavelength, reflecting its contribution to distinguishing water stress levels in rose. PC-1, which captures 77% of the variance, is largely influenced by bands in the near-infrared

region, with strong negative loadings that highlight significant physiological changes under water stress. Key wavelengths with notable loadings on PC-1 include 762.124 nm with a loading of -0.92 , 769.287 nm with -0.91 , and 832.369 nm with -0.94 . These wavelengths are associated with water content and internal leaf structure, both of which are highly sensitive to drought. The negative loadings suggest that as water stress intensifies, there is a shift in reflectance in these bands, likely due to changes in leaf cellular structure and water retention capabilities.

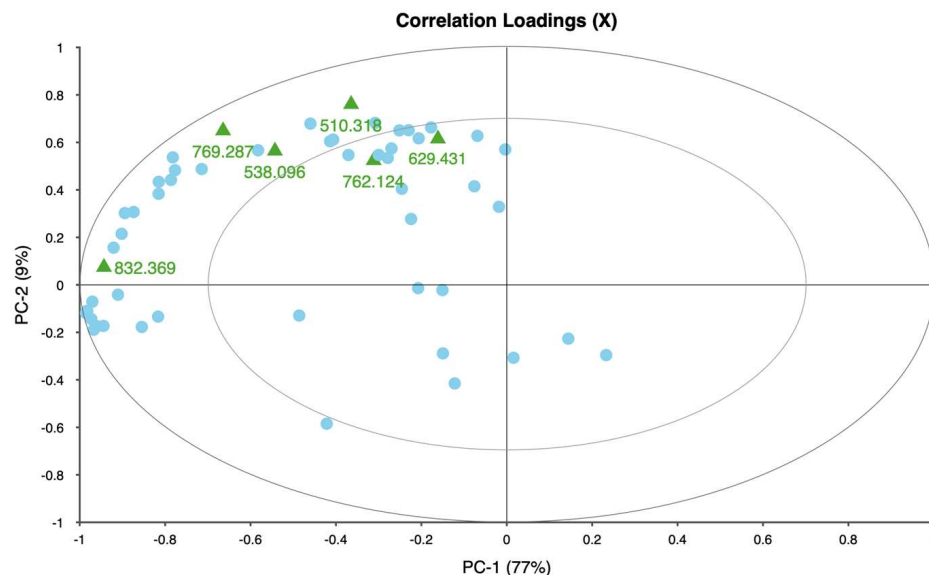


Figure 11. Correlation loadings plot for rose, showing key spectral bands (510.318, 538.096, 629.431, 762.124, 769.287, and 832.369 nm) associated with water stress responses along PC-1 and PC-2.

PC-2, which explains an additional 9% of the variance, is dominated by bands in the visible spectrum, which capture changes related to leaf orientation and pigmentation. Important wavelengths contributing to PC-2 include 510.318 nm with a loading of 0.76, 538.096 nm with 0.56, and 629.431 nm with 0.62. These bands are linked to chlorophyll and other pigments, whose spectral properties change as the plant experiences stress. The positive loadings in these visible bands indicate that early stress responses, such as pigment alteration and chlorophyll degradation, are detectable, offering insights into the initial physiological adjustments to drought stress.

In summary, the correlation loadings analysis identifies essential bands in both the near-infrared (762.124 nm, 769.287 nm, and 832.369 nm) and visible (510.318 nm, 538.096 nm, and 629.431 nm) regions that are critical for distinguishing water stress in rose. These findings underscore the importance of monitoring both water-related structural changes in the near-infrared region and pigment alterations in the visible spectrum. Together, they provide a foundation for developing hyperspectral imaging techniques to detect water stress early in ornamental plants, particularly in rose.

3.1.4. Influence Plot

The influence plot (Figure 12) for rose illustrates the distribution of samples across Hotelling's T^2 values on the x-axis and F -residuals on the y-axis, with data points categorized by day of measurement (D0, D2, D4, and D7) to reflect varying stages of water stress. This visualization reveals the variability and potential outliers within the dataset, providing insight into plant responses under different conditions.

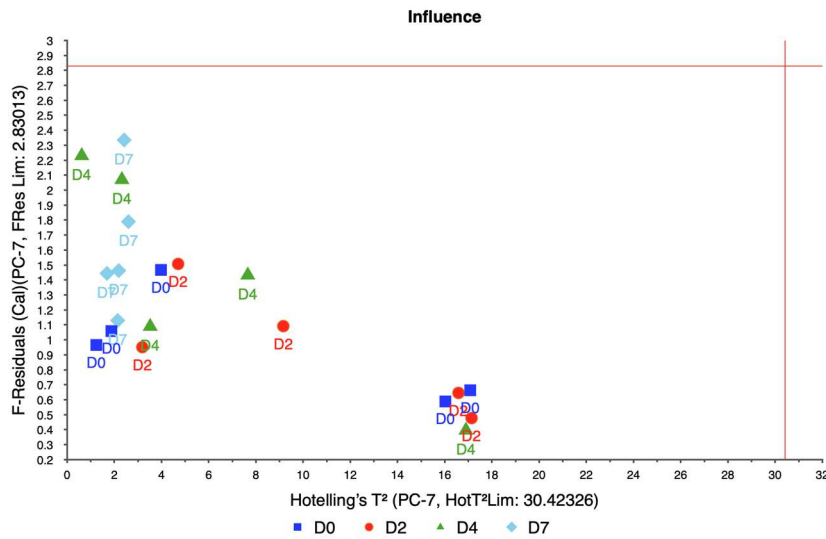


Figure 12. Influence Plot for rose showing sample variability across Hotelling's T^2 and F -residuals, highlighting key outliers under different water stress levels.

Significant points in the plot include samples with high Hotelling's T^2 values, such as Sample 4 (17.14, 0.48) and Sample 8 (17.08, 0.66), which are close to or exceed the confidence limit. These points suggest considerable variance, likely indicating intensified physiological responses under specific stress conditions. The elevated T^2 values highlight samples with more pronounced deviations in response.

Furthermore, samples with moderate Hotelling's T^2 values, such as point 18 (7.65, 1.43), display notable F -residuals, which may reflect nuanced responses at intermediate stress levels. These variations provide a clearer overview and variability in rose's canopy to water stress, pinpointing samples where the spectral data demonstrates the greatest shifts. Rose canopy is layered with smaller leaves creating greater in-canopy variation of spectral response across a given plant. This analysis supports targeted insights into plant resilience and stress adaptation, forming a basis for refining monitoring and management strategies in applications.

The influence plot underscores the importance of carefully considering influential observations in PCA, especially when dealing with complex biological data like plant spectral signatures. By identifying and analyzing these points, researchers can refine their models and improve the accuracy of their conclusions, ultimately leading to a better understanding of how water stress affects rose plants.

3.2. *Itea Virginica*

The PCA conducted on itea data provides insightful information on the variation in spectral signatures associated with different water stress levels over time (D0, D2, D4, D7, representing 0, 2, 4, and 7 days without water).

3.2.1. Explained Variance

The explained variance plot (Figure 13) for itea illustrates how effectively the principal components (PCs) capture the variance in both the calibration and validation datasets. The PC-1 accounts for a significant portion of the variance, explaining 70% for the calibration data and 64% for the validation data. Adding the second component (PC-2) further increases the cumulative variance to 86% for calibration and 78% for validation, indicating that these two components capture the majority of variance in the spectral data. With the third component, the explained variance reaches 92% for calibration and 85% for validation, showing a steady increase. By the fourth principal component, the variance

explained reaches 95% for calibration and 89% for validation. This pattern continues, with diminishing returns from each additional component, eventually reaching 98% for calibration and 91% for validation by the 7th component. This cumulative trend suggests that the model achieves high accuracy with relatively few components, especially within the calibration dataset, indicating that most of the spectral variation in itea, a larger leaf and upright ornamental shrub, is captured efficiently, making it feasible to identify key spectral features related to water stress with a limited number of principal components.

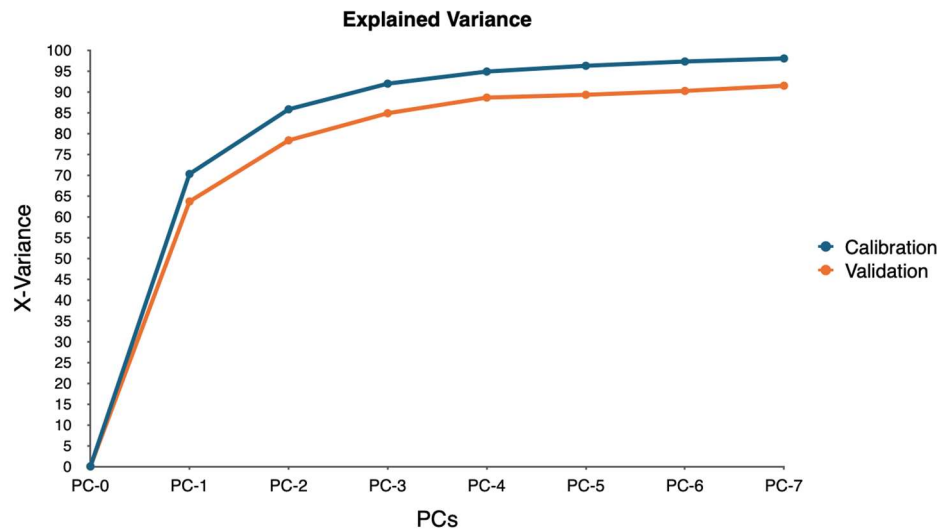


Figure 13. Explained variance plot for itea showing cumulative variance captured by each principal component for calibration and validation datasets.

The cumulative variance explained by PC-1 and PC-2 justifies focusing the analysis primarily on these two components, as they provide a comprehensive summary of the spectral data. This dimensionality reduction is particularly valuable for simplifying complex hyperspectral data, making it easier to visualize and interpret the differences between water stress levels in itea. Moreover, the strong representation of the original data in these two components supports their use in developing predictive models and understanding the physiological responses of plants to water stress.

3.2.2. Score Plot

The Score plot (Figure 14) for itea provides insights into the distribution of different water stress levels over the primary principal components (PC-1 and PC-2). The clusters of points represent various days without water: D0, D2, D4, and D7, showing how itea plants respond to increasing water stress. The spread along PC-1, accounting for 70% of the variance, demonstrates distinct separations between the non-stressed (D0) and stressed groups, with D0 largely clustered on the positive side of PC-1. As stress days increase, the points shift toward the negative side of PC-1, indicating a significant spectral shift under drought conditions. PC-2, which explains 16% of the variance, shows a smaller degree of separation among the days of stress, contributing to a secondary dimension of variability. Together, PC-1 and PC-2 capture the changes in spectral signatures associated with water stress in the canopy of itea, illustrating the crop canopy's response trajectory from no water stress (D0) through to more extended periods of stress (D7). This pattern is useful for identifying specific stages of water stress, with spectral changes becoming more pronounced at higher stress levels.

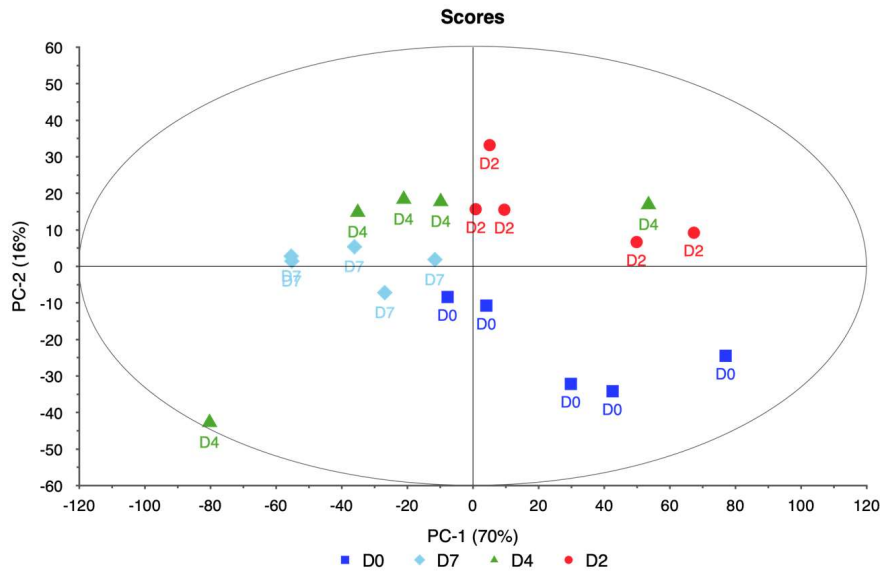


Figure 14. Score plot showing the separation of itea plants by water stress levels (D0, D2, D4, D7) across PC-1 and PC-2.

The clear separation between D0 and the stressed groups (D2, D4, and D7) along PC-1 implies that this component is highly sensitive to the onset of water stress. The increasing spread of points as stress duration increases, particularly along the PC-1 axis, suggests a progressive impact of water stress on the plants' spectral properties.

PC-2, while accounting for less variance than PC-1, captures additional subtleties in the data. The variation along PC-2 might reflect secondary stress responses or differences in plant resilience and adaptation mechanisms that are not captured by PC-1 alone.

3.2.3. Correlation Loadings

The correlation loadings plot (Figure 15) for itea provides an in-depth view of how specific spectral bands contribute to the variation in principal components PC-1 and PC-2, which together explain 86% of the total variance, with PC-1 accounting for 70% and PC-2 for 16%. This substantial explained variance suggests that these two components capture the primary spectral responses associated with water stress in itea. In this plot, the spectral bands are dispersed across the loading space, showing varying degrees of correlation with each principal component. Bands that are closer to the edge of the loading plot have higher correlations with either PC-1 or PC-2, indicating that they play a more substantial role in distinguishing different water stress levels.

In the PC-1 dimension, bands such as 734.46 nm, 762.12 nm, and 769.29 nm contribute strongly to positive loadings. These wavelengths are located in the red-edge and near-infrared regions, which are often linked to chlorophyll concentration and cell structure integrity. Positive loadings at these bands suggest that PC-1 is capturing the spectral characteristics related to changes in leaf angle or structural and compositional changes in the leaf tissues that occur as a response to water stress. These bands are known to shift in reflectance under water-limiting conditions, as the leaf morphology and internal cell arrangement adjust to maintain essential physiological processes despite reduced water availability.

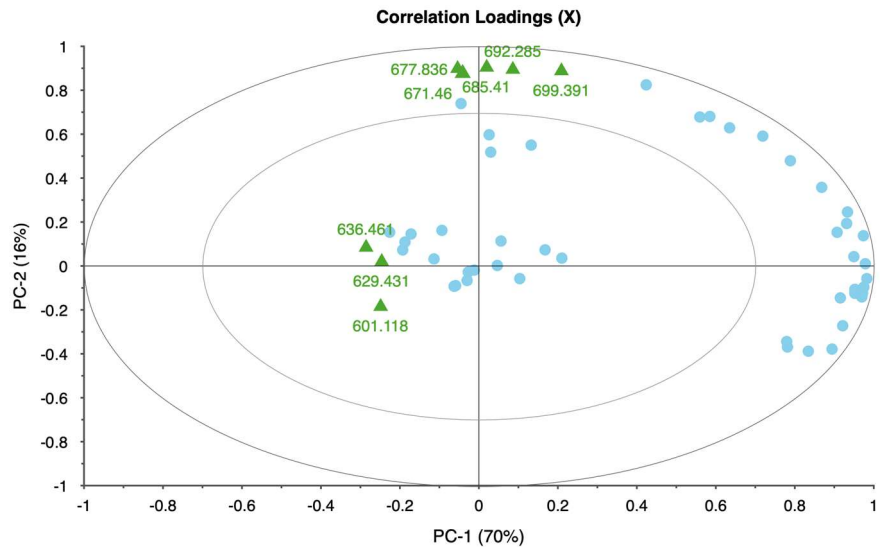


Figure 15. Correlation loadings plot showing the relationship between spectral bands and principal components (PC-1 and PC-2) for itea under varying water stress conditions.

Focusing on the contributions to PC-2, several bands demonstrate strong positive loadings, including those at approximately 671.46 nm, 677.84 nm, 685.41 nm, 692.29 nm, and 699.39 nm. These wavelengths are often associated with key physiological changes, such as changes in chlorophyll fluorescence and pigment concentration, which are sensitive indicators of plant stress. The high positive correlation of these bands with PC-2 suggests that these wavelengths are particularly effective at capturing variations in spectral reflectance as the canopy of itea experiences increasing water stress. These bands may represent areas of the spectrum where chlorophyll absorption decreases, reflecting physiological adjustments as water availability changes. Similarly, bands around 804.23 nm and 811.11 nm show positive loading on PC-2, which may indicate near-infrared reflectance linked to water content within leaf structures, providing further insight into the plant's hydration status under stress.

Conversely, some bands exhibit negative loadings on PC-1 and PC-2, particularly around 601.12 nm, 629.43 nm, and 636.46 nm. These bands, located in the visible region, indicate an inverse relationship with the stress-induced spectral response, which may be associated with changes in light absorption by pigments such as chlorophyll and carotenoids. Under water stress, the changes in pigment concentration and distribution could reduce the reflectance in these bands, leading to the negative loadings observed. This inverse correlation highlights how specific portions of the spectrum respond differently to stress, with certain bands increasing in reflectance while others decrease, painting a complex picture of the plant's adaptation mechanisms.

Together, the correlation loadings plot shows that different regions of the spectrum capture various physiological responses of itea to water stress. The distinct patterns observed in bands across visible and near-infrared regions underscore how stress impacts both the biochemical composition and structural properties of the plants. This analysis reveals that itea plants undergoing water stress exhibit changes that are detectable across specific wavelengths, with certain bands being particularly sensitive indicators of stress conditions. This information is valuable for developing targeted monitoring approaches that leverage these key wavelengths to assess plant health in ornamental species under water-limited environments. By identifying these significant bands, this study advances the understanding of how spectral data can be used to monitor stress-related changes in plants, contributing to improved management and conservation practices in nursery production.

3.2.4. Influence Plot

The influence plot (Figure 16) for *itea*, based on PC-4, provides valuable insights into the spectral response of *itea* plants to varying levels of water stress over time. This plot displays *F*-residuals on the y-axis and Hotelling's T^2 values on the x-axis, with a threshold line indicating the limits for acceptable influence. Each data point is labeled according to the days of water stress experienced by the plants (D0, D2, D4, and D7), representing the progression of stress conditions from well-watered (D0) to seven days without water (D7).

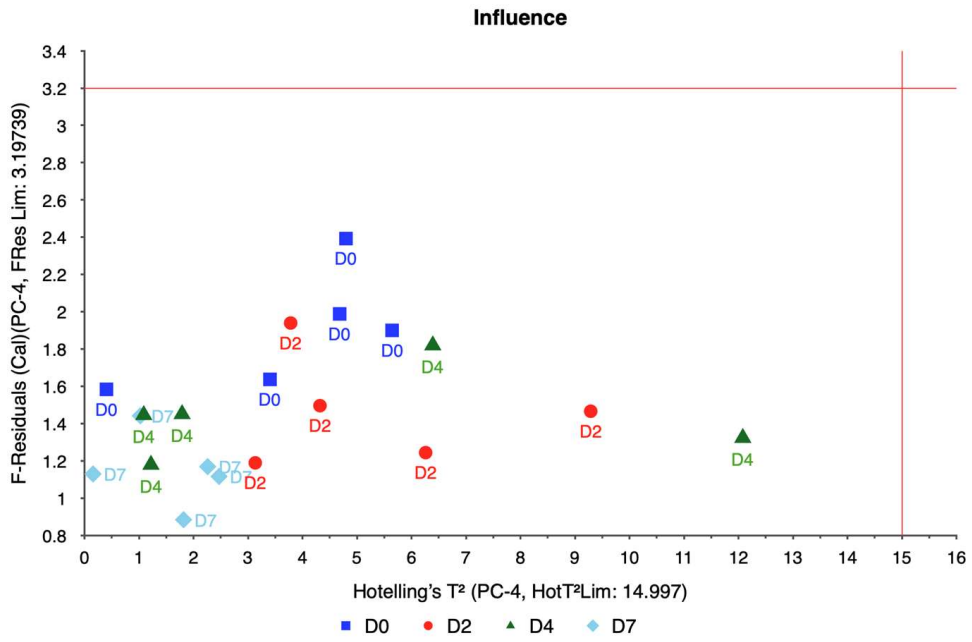


Figure 16. Influence plot for *itea* showing the impact of varying water stress levels across different days (D0, D2, D4, D7) on spectral response, with notable deviations at the D4 stage.

Upon examination, most data points fall within the acceptable bounds of Hotelling's T^2 limit, indicating they are not exerting undue influence on the model and are relatively consistent with the expected spectral response patterns. The majority of points from D0, D2, and D7 are clustered near the center, indicating minimal deviation in their response under these conditions. This suggests that plants at the initial (D0) and longer-term (D7) stages of stress maintain a relatively stable response within the model's scope.

However, a subset of points, primarily from day D4, exhibit Hotelling's T^2 values approaching or surpassing the threshold, showing a high degree of influence. This shift implies that the plants at D4, a middle stage of water stress, exhibit notable changes in their spectral signature, potentially indicative of physiological adjustments or stress responses that differ from those at the initial and prolonged stress stages. These D4 points often coincide with elevated *F*-residual values, highlighting the increased variability in spectral data during this period of moderate stress, possibly due to variations in available water, leaf and whole-canopy turgor, leaf structure, and other physiological responses.

Interestingly, the presence of a few outlier points—especially from D4—underscores the variability in the water stress response of *itea* leaf and whole canopy. This variability at the intermediate stress level (D4) could reflect transitional physiological changes as the plants adapt to a decrease in water availability and subsequent decrease in plant water potential. In contrast, the points from D0 and D7 suggest either an absence of stress (D0) or a possible acclimatization to prolonged stress conditions (D7), where the plants may have reached a stabilized response pattern.

Overall, the influence plot for *itea* highlights the significant spectral shifts occurring around D4, marking it as a critical point of transition in the plants' response to water

stress. This finding aligns with the concept that plants may exhibit more pronounced physiological changes at intermediate stages of stress, as opposed to either the onset (D0) or extended duration (D7) of water deprivation. These insights are crucial for understanding the temporal dynamics of *itea*'s response to drought conditions and may aid in refining water stress monitoring techniques for early detection and intervention in containerized ornamental plant production.

3.3. *Spirea*

The PCA for spirea aims to explore how spectral signatures of the plants change under varying levels of water stress. The water stress levels are represented by the number of days without water (D1, D2, D4, and D7, corresponding to 1, 2, 4, and 7 days, respectively). This analysis focuses on identifying the key spectral bands contributing to the observed variations and understanding how these changes reflect the physiological responses of spirea to water stress.

3.3.1. Explained Variance

The explained variance plot (Figure 17) for spirea shows how each PC contributes to the overall variance captured in the calibration and validation datasets. For the calibration set, PC-1 explains 74% of the variance, with cumulative explained variance reaching over 90% by PC-2 (91%) and over 94% by PC-3 (94.51%). This indicates that the majority of the spectral data variability can be explained by the first three components, demonstrating that they capture essential information about spirea's response to water stress.

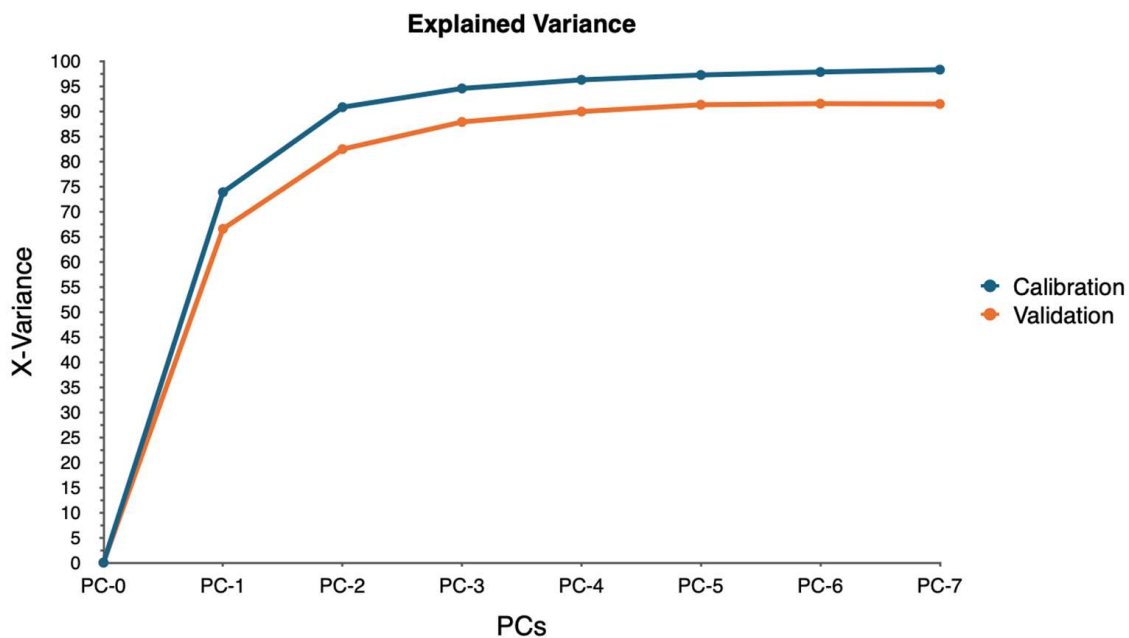


Figure 17. Explained variance plot for spirea, showing cumulative variance captured by each principal component in calibration and validation datasets, with over 90% variance explained by the first three components.

In the validation dataset, the explained variance follows a similar trend, with PC-1 capturing 67% and cumulative variance exceeding 82% by PC-2 (82.41%) and reaching 88% by PC-3. Although slightly lower than the calibration set, the validation results indicate that these components still effectively represent the data variability, confirming the model's robustness across both calibration and validation datasets.

3.3.2. Scores Plot

The score plot (Figure 18) for spirea illustrates the distribution of spectral responses to varying water stress levels, represented along the first two principal components, PC-1 and PC-2, which together capture 91% of the total variance (74% and 17%, respectively). This high cumulative variance suggests that these components effectively encapsulate the main spectral variations associated with water stress in spirea. PC-1, which accounts for the majority of the variance, shows a notable spread from positive to negative values. Points representing lower stress levels (D1 and D2) are clustered toward the positive end of PC-1, while higher stress levels (D4 and D7) shift towards more negative values. This gradient along PC-1 indicates that this component primarily reflects physiological changes due to increasing water stress, with positive scores likely corresponding to minimal stress response and negative scores indicating a progressive intensification of water stress. These changes could be associated with reduced water content, alterations in chlorophyll levels, or structural modifications in leaf tissues as drought conditions persist over time.

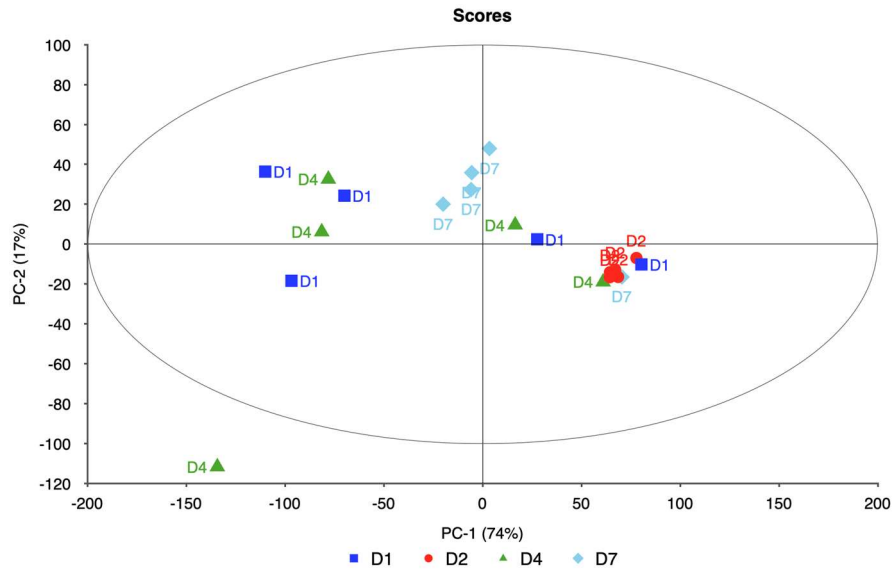


Figure 18. Score plot for spirea showing the distribution of spectral responses across water stress levels, with PC-1 capturing primary stress indicators and PC-2 reflecting secondary physiological changes.

In contrast, PC-2, although explaining a smaller portion of the variance, captures secondary physiological responses to prolonged water stress. Points associated with D4 and D7, which represent more extended drought exposure, exhibit a wider spread along PC-2 compared to D1 and D2, which are more tightly clustered. This pattern suggests that as water stress endures, additional physiological variations emerge, potentially due to adaptive or stress-mitigation mechanisms. These could include adjustments in pigment composition, leaf structural changes, or shifts in metabolic processes that become more pronounced in the later stages of stress. The clustering of D1 and D2 data points indicates a relatively consistent response pattern during early water stress with minimal spectral variation, while the broader dispersion of D4 and D7 reflects greater variability, which could be attributed to differences in individual plant tolerance or the onset of adaptive physiological changes.

Overall, the score plot underscores the sensitivity of spirea to water stress, with PC-1 capturing primary indicators of stress severity and PC-2 identifying more complex, secondary responses. This analysis provides a comprehensive view of how spirea's spectral

signature evolves under drought conditions, offering insights into early and progressive indicators of stress.

3.3.3. Correlation Loading Plot

The analysis of correlation loadings (Figure 19) for spirea under water stress conditions provides insight into key spectral bands that reveal physiological responses. Principal Component 1 (PC-1), which explains 74% of the variance, is heavily influenced by bands in the visible to near-infrared range. Notably, high positive loadings in PC-1 are observed at wavelengths around 650.386 nm, 657.145 nm, 664.373 nm, and 671.46 nm. These bands, primarily within the red and near-infrared regions, are closely associated with chlorophyll absorption, indicating that water stress may induce changes in chlorophyll content or leaf pigmentation. This suggests that chlorophyll-related spectral features are strong indicators of early water stress in spirea, as they exhibit high sensitivity under drought conditions.

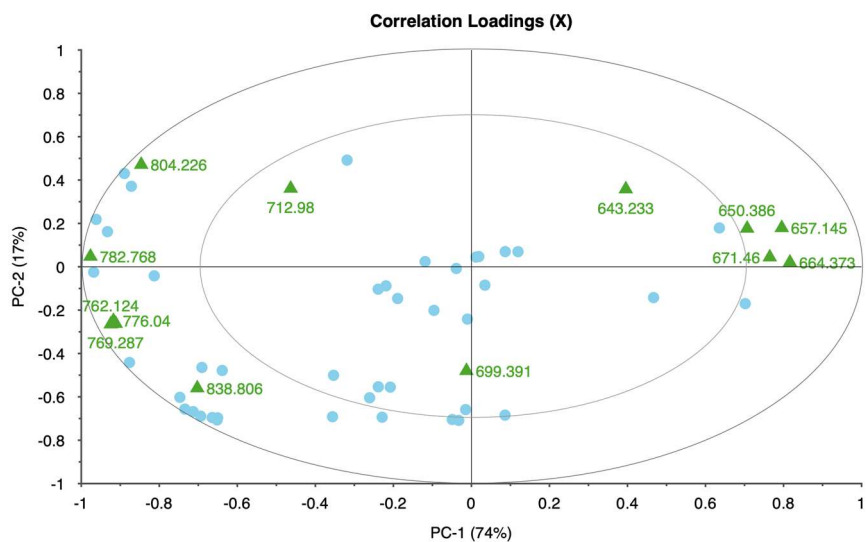


Figure 19. Correlation loadings plot for spirea under water stress, highlighting key spectral bands associated with chlorophyll content (positive loadings) and leaf structure changes (negative loadings).

In contrast, PC-1 also shows strong negative loadings at wavelengths around 762.124 nm, 769.287 nm, 776.04 nm, and 782.768 nm, which fall within the near-infrared range. This region is commonly associated with leaf structure and water turgor. The negative correlation at these wavelengths suggests that water stress may be altering the internal leaf structure, likely due to reduced cell wall integrity. These changes in structural integrity are reflected as a decrease in near-infrared reflectance, a known indicator of water loss in plant tissues.

PC-2, which explains 17% of the variance, captures additional spectral changes less directly related to primary water stress responses. Positive loadings are observed at wavelengths such as 643.233 nm, 712.98 nm, and 804.226 nm. These bands could reflect secondary physiological responses, possibly related to pigment adjustments or slight structural shifts that occur as stress progresses. The near-infrared band around 804.226 nm, in particular, may indicate subtle changes in leaf structure beyond those primarily captured by PC-1.

Moderate negative loadings in PC-2 at wavelengths like 699.391 nm and 838.806 nm suggest that certain spectral features may exhibit an inverse relationship with secondary stress responses. These bands may represent aspects of spirea's change in physiological state that either counterbalance or do not correlate directly with primary water stress indicators.

Overall, the correlation loadings for spirea emphasize the sensitivity of specific red and near-infrared bands to water stress, with PC-1 capturing primary stress responses

linked to chlorophyll and structural integrity, while PC-2 reflects more nuanced secondary responses. These findings underscore the utility of hyperspectral imaging in detecting early signs of water stress in ornamental plants and highlight key spectral bands that can inform water management strategies for spirea.

3.3.4. Influence Plot

The influence plot (Figure 20) for spirea illustrates the distribution of data points based on their Hotelling's T^2 values and F -residuals on PC-5, which measures each point's leverage and distance from the model center. This plot provides insights into outliers and high-influence points, potentially indicating unique variations in spectral response of spirea canopy to water stress across different time intervals (D1, D2, D4, and D7). Most data points fall within the acceptable influence limits, with relatively low Hotelling's T^2 and F -residual values, suggesting alignment with the overall model and indicating consistent spectral responses to water stress. However, a few points—notably one with a Hotelling's T^2 value of 15.89—show higher leverage, suggesting significant deviations from the expected pattern.

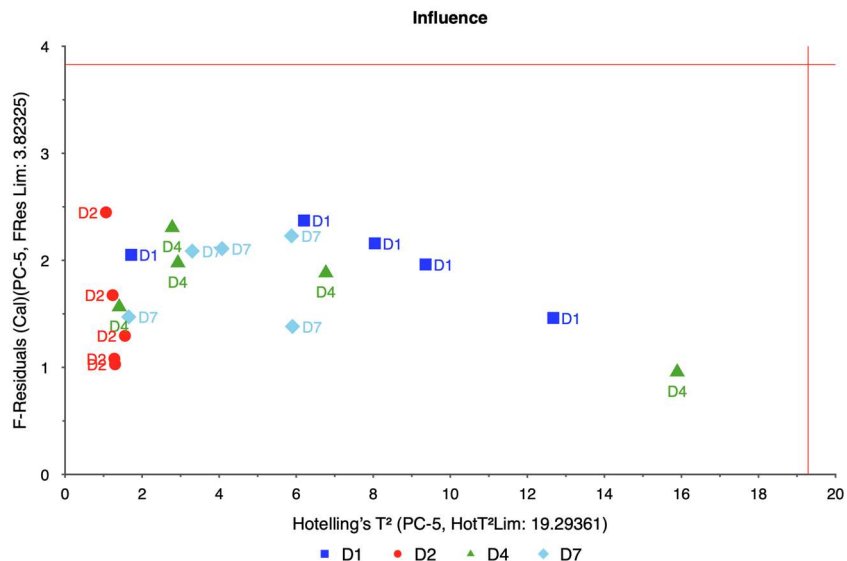


Figure 20. Influence plot for spirea, showing data point leverage and variation in spectral response under increasing water stress levels, with higher influence observed in prolonged drought conditions (D4 and D7).

Points from earlier days (D1 and D2) generally exhibit lower Hotelling's T^2 and F -residual values, reflecting a predictable spectral response during the initial stages of water stress. As stress continues over time, data points from days D4 and D7 display greater variation, with a broader spread in influence values. The physiological variation across measured spirea canopies under prolonged water stress. Similar to rose, spirea is a small leaf canopy constructed of layers of leaves. However, the canopy is much tighter, overlapping than rose. The increased influence of these later points highlights how cumulative water stress can lead to distinct and variable spectral characteristics.

Overall, the influence plot underscores the progressive nature of canopy response of spirea to extended drought conditions. The presence of higher-influence points among D4 and D7 data suggests that PC-5 captures secondary responses to water stress, which become more pronounced over time. This analysis helps identify specific instances of physiological change, which can be used to refine predictive models for detecting water stress in container grown spirea and similar produced ornamental species with like canopy

and leaf morphology. It should be noted that plant provenance could further play a role in individual species' drought resistance.

3.4. Weigela

The PCA for weigela explores the spectral responses of the plant under different water stress levels over time. The stress levels are represented by the number of days without water: D0 (0 day), D1 (1 day), D3 (3 days), and D5 (5 days). This analysis focuses on identifying the key spectral bands that contribute to the variance observed across these stress levels and understanding how these changes reflect the physiological responses of weigela to water stress.

3.4.1. Explained Variance

The explained variance plot (Figure 21) for weigela provides insights into the distribution of variance across PCs for both calibration and validation datasets. As illustrated in the first three principal components account for a significant proportion of the total variance. For the calibration data, PC-1 alone explains 50% of the variance, which increases cumulatively to 71% by PC-2 and 82% by PC-3. This is the lowest percent of explained variance across taxa; possibly due to the three-color blooms that were lightly present during hyperspectral analysis. The explained variance continues to rise steadily with each additional component, reaching a cumulative 96% by PC-7, indicating that most of the data's variability is captured within these components.

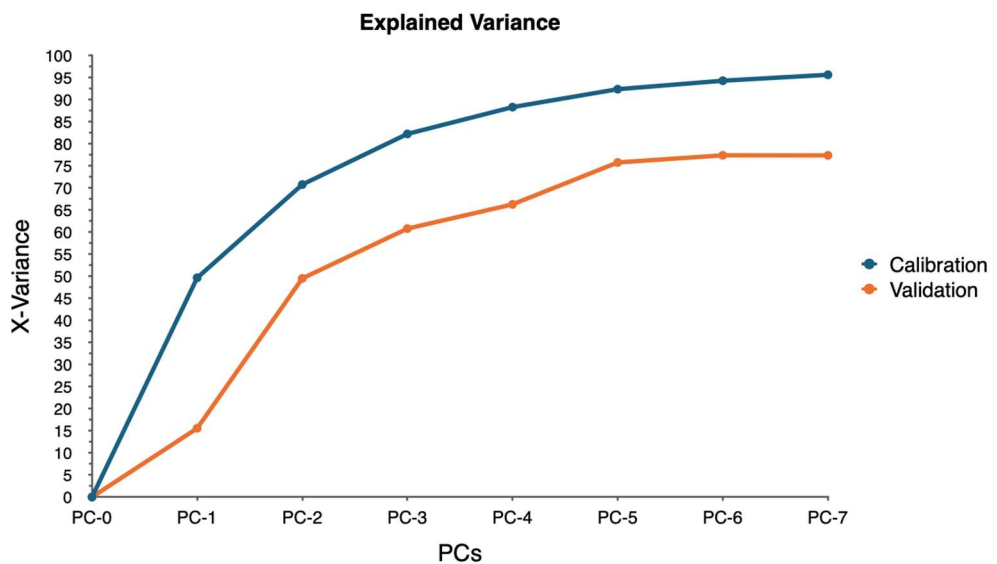


Figure 21. Explained variance plot for weigela showing cumulative variance captured by each principal component for calibration and validation datasets.

In the validation dataset, a similar trend is observed but with slightly lower explained variances, signifying a minor drop in predictive accuracy. PC-1 explains 16% of the variance, which grows to 50% by PC-2 and 61% by PC-3. By PC-7, the cumulative variance reaches 77%. This difference between calibration and validation datasets highlights some degree of model variability, possibly indicating the model's sensitivity to variations in data or suggesting further refinement for optimal predictive performance.

This explained variance distribution underscores the importance of the initial few components in capturing the primary variance within the weigela dataset, with calibration data providing a strong foundation for the model, while validation data reveal areas where predictive robustness could be improved.

3.4.2. Scores Plot

The scores plot (Figure 22) for weigela provides insights into the spectral differentiation among specimens subjected to varying levels of water stress over time. PC-1, which explains 50% of the total variance, effectively separates the well-watered (D0) samples from those experiencing water deprivation. Samples under the D0 condition, represented by blue squares, predominantly cluster on the positive side of the PC-1 axis, indicating a unique spectral profile associated with sufficient hydration. In contrast, samples exposed to water stress conditions, particularly D3 (three days without water) marked by green triangles, show a clear shift towards the negative side of PC-1, reflecting substantial changes in spectral properties as a result of water deficit.

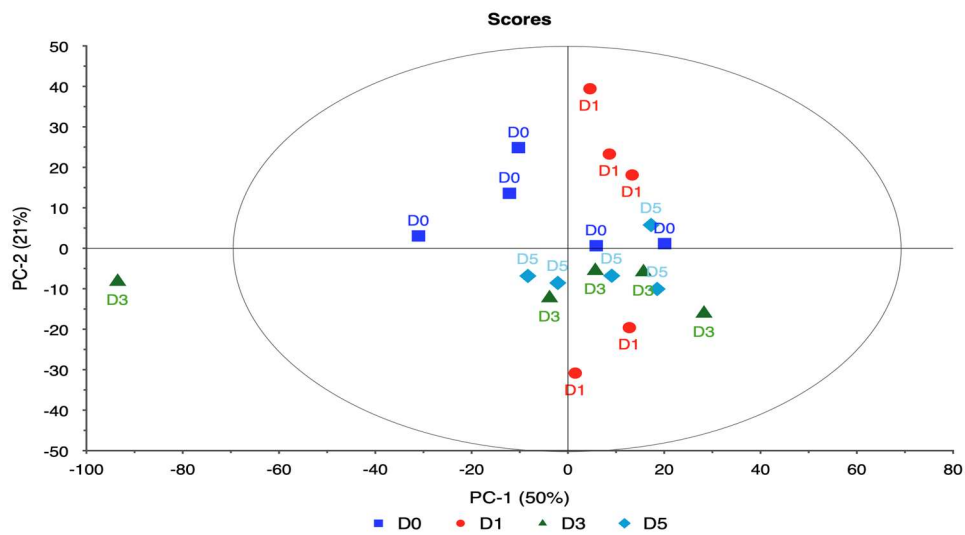


Figure 22. Scores plot for weigela showing the separation of samples under different water stress levels along PC-1 and PC-2.

PC-2, which accounts for an additional 21% of the variance, further distinguishes the samples based on nuanced variations within each water treatment level. For instance, D1 (one day without water) and D5 (five days without water) samples display wider dispersion along both PC-1 and PC-2, highlighting a range of spectral responses within these stress levels. The dispersion across PC-2 suggests that while PC-1 captures the primary impact of water availability on spectral characteristics, PC-2 may be reflecting secondary factors such as minor physiological or biochemical changes in response to stress.

The plot reveals that as the duration of water stress increases, the weigela leaves and canopies exhibit increasingly distinct spectral signatures, forming clusters that correspond to the level of water deprivation. The separation along PC-1 and the spread along PC-2 emphasize how water stress influences the plant's spectral response, with greater stress levels yielding more marked divergence from the well-watered baseline. This analysis indicates that PCA effectively captures the progression of water stress in weigela, aiding in the understanding of how spectral data can reflect physiological changes due to drought conditions.

3.4.3. Correlation Loading Plot

The correlation loadings plot (Figure 23) for water stressed canopy of weigela provides a detailed view of the influence of various spectral bands on the primary components extracted during PCA, specifically PC-1 and PC-2. Together, these components account for a substantial portion of the variability within the spectral data, with PC-1 contributing 50% and PC-2 adding an additional 21%. This cumulative variance reflects the complexity

and variability of the weigela samples' spectral responses under varying conditions, such as water stress.

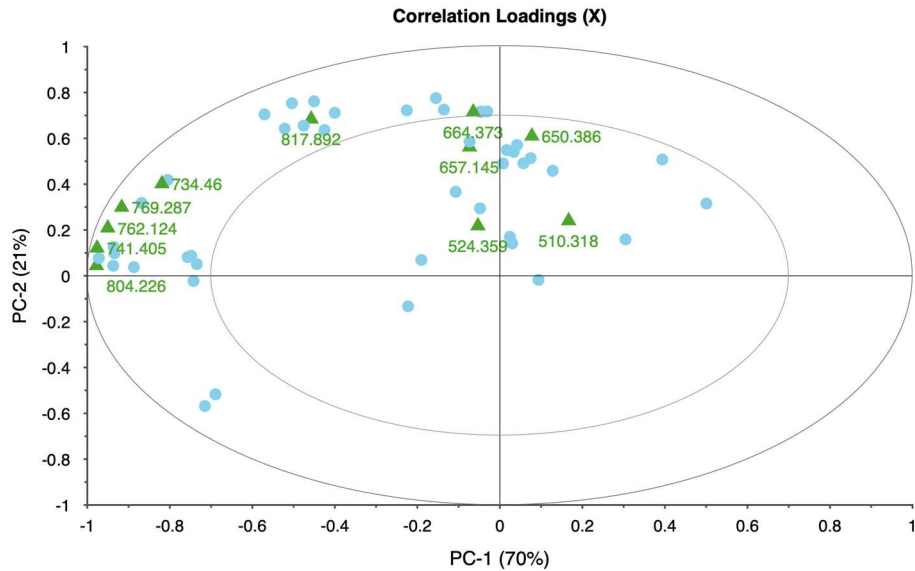


Figure 23. Correlation loadings plot for weigela showing the influence of different spectral bands on the first two principal components (PC-1 and PC-2), highlighting key wavelengths contributing to data variance and structure.

In examining the individual bands, notable patterns emerge. Spectral bands around 510.318 nm and 524.359 nm show moderate contributions to PC-1, indicating a balanced influence on data structure in both directions. These bands also have high loadings on PC-2, suggesting that they may capture specific variations that are distinct from the primary variance trend represented by PC-1. Bands within the visible red to near-infrared region—such as 650.386 nm, 657.145 nm, and 664.373 nm—exhibit high positive loadings on both PC-1 and PC-2, marking them as significant contributors to the overall variance. This high loading indicates that these wavelengths are particularly sensitive to changes within the weigela leaf physiology when loss of turgor, potentially correlating with physiological responses to water stress.

Some bands, such as 734.46 nm and 741.405 nm, show strong negative loadings on PC-1 but moderate positive or neutral loadings on PC-2. These inverse contributions suggest that these wavelengths capture unique characteristics within the data, potentially representing physiological markers that behave differently under stress. Such variations in spectral loadings emphasize the differential responses of weigela to environmental conditions, which are represented by the diverse impacts across these specific bands.

Other high-loading bands, including those around 762.124 nm and 769.287 nm, reinforce the role of near-infrared wavelengths in detecting structural or water-related stress in weigela. These bands' high loading values on PC-1 and moderate contributions to PC-2 highlight their importance in capturing changes within the plant tissue, likely due to shifts in cellular water content or other stress indicators. Additionally, some bands in the upper wavelengths, like 804.226 nm and 817.892 nm, exhibit high positive loadings on PC-1 and moderate on PC-2, emphasizing the contribution of near-infrared spectral information.

The correlation loadings plot illustrates the critical spectral regions influencing the dataset, allowing researchers to pinpoint specific wavelengths that are likely indicators of physiological or stress-related changes in the foliage of weigela. This understanding not only aids in the interpretation of hyperspectral data but also guides future monitoring efforts by identifying wavelengths that serve as reliable markers for assessing plant health and stress responses. This plot serves as a foundational tool in linking spectral signatures

to physiological states, reinforcing the importance of PCA in hyperspectral analysis for monitoring ornamental plant health.

3.4.4. Influence Plot

The influence plot (Figure 24) for weigela provides an in-depth view of the variation and influence of data points in the PCA model, specifically focusing on the PC-6. In this plot, Hotelling's T^2 (along the x-axis) and F -residuals (along the y-axis) reveal the degree of influence each observation exerts on the PCA model, highlighting potential outliers or influential points. Data points for various days (D0, D1, D3, D5) reflect the plant's responses to water stress over time, with distinct groupings indicating the differing levels of influence exerted by each individual canopy at different time intervals.

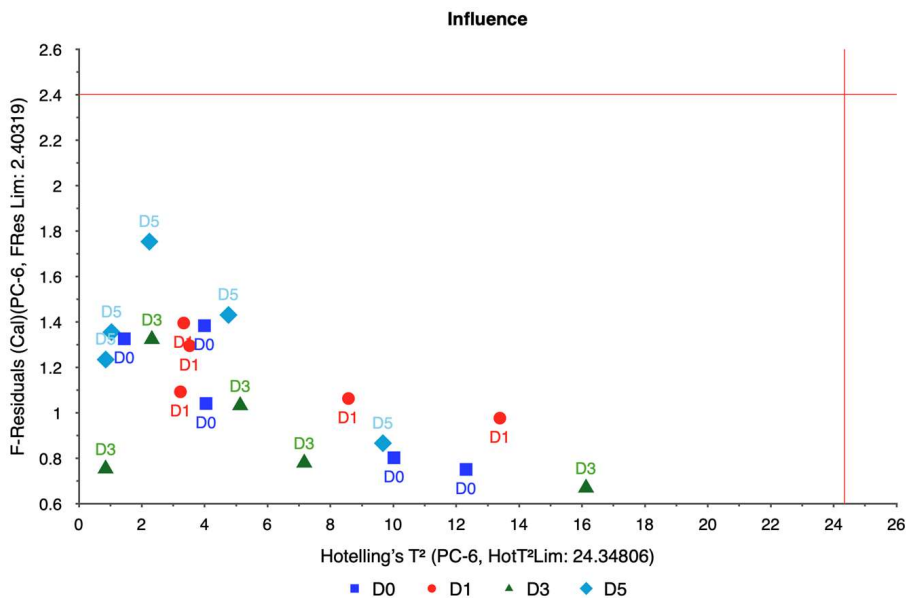


Figure 24. Influence Plot for weigela showing Hotelling's T^2 against F -residuals for PC-6, highlighting influential data points and identifying outliers across different days under water stress conditions.

From the data, observations with Hotelling's T^2 values closer to the upper threshold of 24.34806 represent more influential observations in the PCA model structure. For instance, observations with Hotelling's T^2 values between 10 and 16 suggest moderate influence, while points like D0, D1, and D5 stay within safe limits. On the F -residual axis, values range up to around 2.4, marking the threshold for identifying outliers. Notably, data points near this threshold warrant further investigation, as they may signify significant variances or anomalies in the spectral response due to water stress, canopy structure, flower interference, or leaf angle and structure. Overall, this influence plot aids in isolating points that could affect model reliability, ensuring that the dataset used for analysis remains robust and accurately represents weigela's physiological response to water stress.

4. Discussion

This study focused on evaluating the spectral responses of four ornamental plant taxa—rose, itea, spirea, and weigela—under varying levels of water stress using hyperspectral imaging combined with PCA. The goal was to identify key spectral bands associated with water stress and to assess the potential of these bands for early detection and monitoring of plant health as shown in Table 2.

Table 2. Summary table of results for each taxa.

Taxa	Key Spectral Bands	Explained Variance (PC-1 + PC-2)	Main Observations
<i>Rosa</i> (rose)	650.386, 692.285, 734.460, 762.124	77% + 9% = 86%	High sensitivity to water stress in the red and near-infrared bands; distinct clustering observed in score plot for stressed vs. non-stressed samples.
<i>Itea virginica</i> (itea)	664.373, 685.410, 706.114, 727.202	70% + 16% = 86%	Moderate separation in response to water stress; influence plot reveals significant variability at early stages of water deficit.
<i>Spiraea nipponica</i> (spirea)	643.233, 677.836, 711.460, 734.460	74% + 17% = 91%	Clear differentiation in spectral responses to stress, with notable shifts in reflectance at 643–734 nm. Correlation loadings show strong response in near-infrared bands.
<i>Weigela florida</i> (weigela)	636.461, 664.373, 692.285, 762.124	50% + 21% = 71%	Most affected by water stress among taxa; substantial changes in near-infrared reflectance with prolonged stress. High variability in influence plot, suggesting diverse response patterns.

Each taxon exhibited distinct patterns in reflectance across spectral bands, demonstrating unique physiological adaptations and responses to water deficits. Rose displayed significant changes in the red and near-infrared regions, specifically at 650.386, 692.285, 734.460, and 762.124 nm. These shifts in reflectance were strongly associated with water stress, allowing for clear differentiation between stressed and unstressed samples. The high explained variance achieved in rose's principal components analysis suggests that these spectral bands reliably captured the effects of water stress, making rose a responsive model for studying drought sensitivity in ornamental plants.

In itea, the spectral bands at 664.373, 685.410, 706.114, and 727.202 nm showed noticeable reflectance changes, especially in the early stages of water stress. While itea's response was moderate compared to rose, the high explained variance in its PCA indicates that the selected spectral bands were effective in capturing the initial impact of water stress. This finding is significant for early detection of stress in nursery settings, where timely intervention could mitigate potential growth or quality impacts on itea plants.

The spirea's spectral response was pronounced in the near-infrared bands, with key shifts observed at 643.233, 677.836, 711.460, and 734.460 nm. These bands allowed for robust differentiation of stress levels, as evidenced by the model's high reliability. The distinct spectral changes observed in spirea suggest that it may be well-suited for hyperspectral stress monitoring, particularly for identifying moderate to severe stress levels. The explained variance for spirea further supports the accuracy of the spectral data in capturing water stress indicators.

The weigela showed the most varied response to water stress among the four taxa, with key spectral bands located at 636.461, 664.373, 692.285, and 762.124 nm. This variation suggests a heightened sensitivity to prolonged water deficits, as reflected in the influence plot where a wider distribution of data points was observed. The high variability in weigela's spectral response highlights its diverse physiological responses to drought stress. Weigela's results underscore the importance of using a multi-band approach to fully capture its stress dynamics, making it a potentially complex model for monitoring plant health under drought conditions.

The differences in spectral responses across taxa can be attributed to their unique physiological adaptations to drought. For instance, rose exhibited higher sensitivity due to its limited water-holding capacity and greater reliance on stomatal regulation. In contrast, weigela demonstrated a broader range of stress responses, likely due to its robust root system and efficient water use strategies. These physiological differences explain the taxa-specific patterns observed in the spectral bands and highlight the importance of considering plant morphology and drought tolerance in hyperspectral studies.

While PCA proved effective in reducing the dimensionality of hyperspectral data and identifying key spectral bands associated with water stress, the method has inherent limitations and assumptions that must be considered. First, PCA assumes linear relationships between variables, which may not fully capture the complex, non-linear interactions present in biological systems such as plants. This assumption could limit the interpretability of certain principal components, especially when non-linearities dominate the spectral data. Second, PCA is sensitive to noise, which can disproportionately affect the derived components and potentially obscure meaningful patterns. In this study, rigorous pre-processing steps, including radiometric and geometric corrections and the removal of outliers, were employed to minimize noise and ensure the reliability of the analysis. Finally, the interpretability of principal components can be challenging, as they represent linear combinations of original variables that may not directly correspond to specific biological traits. This underscores the importance of coupling PCA with domain knowledge to relate spectral data to physiological plant responses accurately.

The identified spectral bands (e.g., 762 nm and 810 nm) have significant implications for practical water management in horticultural settings. For irrigation scheduling, these bands can serve as early indicators of water stress, enabling nursery operators to implement precision irrigation strategies. Monitoring reflectance at these wavelengths allows for stress detection before visible symptoms appear, optimizing the timing and amount of water applied. This can result in significant water savings and improved plant health.

Furthermore, the taxa-specific spectral responses observed in this study provide a foundation for adaptive water management strategies. For instance, *Rosa hybrid*, which exhibited significant stress signals at key bands, may require more frequent or targeted irrigation. In contrast, *Weigela florida*, with its broader stress tolerance, can be managed with interventions like mulching or shading to reduce water loss. These approaches enhance water use efficiency while maintaining plant quality and marketability in ornamental nurseries. Comparisons with recent studies, such as Virnodkar et al. and Wong et al., highlight the potential of hyperspectral imaging in distinguishing water stress responses across different taxa [19,20]. While these studies focus on agricultural crops, their findings support the broader application of hyperspectral imaging in precision agriculture. This alignment underscores the value of extending these methodologies to ornamental species, as demonstrated in our research.

These findings highlight the potential of hyperspectral imaging as a non-invasive tool to integrate into real-world horticultural practices, contributing to sustainable water management and improved drought resilience. The taxa-specific spectral responses observed in this study, particularly in the red and near-infrared regions, provide unique insights into the physiological changes associated with water stress. These findings not only contribute to the limited body of knowledge on hyperspectral imaging in ornamental species but also highlight the potential for broader applications in precision nursery management.

The findings of this study align with recent research demonstrating the capability of hyperspectral imaging for stress detection in agriculture. For example, Osco et al. highlighted the potential of hyperspectral indices derived from artificial neural networks for identifying water stress in lettuce under controlled conditions [15]. Similarly, Nagasubra-

manian et al. showcased the efficacy of hyperspectral imaging integrated with 3D deep learning in detecting plant diseases [17]. Unlike these studies, which focus on food crops, our work extends this technology to ornamental plants, representing a novel application with economic and aesthetic significance.

The study's findings emphasize the utility of hyperspectral imaging as a tool for detecting water stress in ornamental plants. The species-specific responses across rose, itea, spirea, and weigela suggest that while each taxon responds differently to water stress, key spectral bands in the red and near-infrared regions serve as reliable indicators across all taxa. The high explained variance in each taxa's PCA results supports the robustness of the spectral data in capturing stress indicators. Overall, hyperspectral imaging enables precise monitoring of water stress, providing insights for nursery management and drought resilience in ornamental plant production.

5. Conclusions

This study demonstrates that hyperspectral imaging, combined with PCA, provides a powerful approach for detecting and monitoring water stress in ornamental plants. The spectral responses of four ornamental woody shrub taxa produced in 11 L containers revealed distinct, species-specific patterns across key bands in the red and near-infrared regions. These bands—such as 650.386, 664.373, 692.285, and 734.460 nm—proved effective in distinguishing between stress levels, highlighting the potential of hyperspectral data for early and accurate stress detection in containerized nursery crop production. The high explained variance across taxa further supports the robustness and reliability of these spectral indicators, emphasizing the value of hyperspectral imaging in precision agriculture for ornamental species.

While the findings underscore the ability of hyperspectral imaging to identify water stress in these four taxa, future research should focus on expanding the scope of this approach to other ornamental plant species and environmental stress factors. Investigating how different plant varieties within the same taxa respond to stress could provide more nuanced insights into species resilience. Additionally, integrating hyperspectral data with other physiological measurements, such as leaf water potential and stomatal conductance, may enhance the understanding of the underlying mechanisms driving spectral changes. Exploring machine learning techniques to complement PCA could improve the ability to analyze non-linear relationships in hyperspectral datasets, potentially increasing the accuracy and applicability of stress detection.

This study was conducted in a controlled environment, which, while advantageous for isolating water stress variables, may not fully replicate the variability present in real-world nursery settings. Future research should validate these findings under field conditions to ensure robustness across diverse environments. Furthermore, the sensitivity of PCA to noise and its linearity assumption may limit the interpretation of spectral data. Additional studies incorporating advanced computational approaches or combining hyperspectral imaging with other technologies could address these limitations.

Research on real-time, field-based hyperspectral imaging systems would also be beneficial, as it would allow for continuous monitoring of plant health in dynamic nursery environments. Ultimately, integrating hyperspectral imaging into operational nursery practices has the potential to revolutionize water management strategies, enabling more sustainable and efficient production of ornamental plants.

Author Contributions: Conceptualization, J.M.M., V.P., J.N., J.R., J.O.J., J.B., D.B., I.B.-S., A.d.C. and J.M.P.; methodology, V.P., J.N., J.M.M., J.R., J.O.J., J.B. and D.B.; software, V.P., J.N., J.M.M., J.O.J. and J.R.; validation, V.P., J.N., J.M.M. and J.R.; formal analysis, V.P., J.N., J.M.M., J.O.J. and J.R.; investigation, V.P., J.N., J.M.M., J.R., J.O.J., J.B., D.B., I.B.-S., A.d.C. and J.M.P.; resources, J.M.M., J.R., J.O.J., J.B. and D.B.; data curation, V.P., J.N., J.M.M., J.R., J.O.J., J.B. and D.B.; writing—original draft preparation, V.P., J.M.M., J.O.J. and J.R.; writing—review and editing, V.P., J.N., J.M.M., J.R., J.O.J., J.B., D.B., I.B.-S., A.d.C. and J.M.P.; visualization, V.P. and J.M.M.; supervision, J.M.M., J.O.J. and J.R.; project administration, J.M.M. and J.R.; funding acquisition, A.d.C., J.M.P. and J.M.M. All authors have read and agreed to the published version of the manuscript.

Funding: This research was funded by the following: J. Frank Schmidt Family Charitable Foundation 2018000384 Award 247, ECOdigital project (ref. MMT24-ICA-01) of the MOMENTUM CSIC program and TED2021-132401A-I00 (PRTR and European Union-NextGenerationEU), PID2023-150108OB-C31, and PID2023-150108OB-C32 from the Spanish MCIU/AEI/10.13039/501100011033 and FEDER, EU. Research of Dr. Peña was financed by the “Salvador de Madariaga” for Visiting Researchers in Foreign Centers Program (Spanish MICINN funds). The research of IBS was financed by the grant FJC2021-047687-1, funded by MCIN/AEI/10.13039/501100011033 and European Union NextGenerationEU/PRTR.

Data Availability Statement: The original contributions presented in the study are included in the article, further inquiries can be directed to the corresponding author.

Acknowledgments: We would like to express our sincere gratitude to Julie Brindley, and Anna Paulk for their crucial help in the preparation of the plants and their dedicated efforts during the fieldwork. Their contributions were essential to the success of this study, and we greatly appreciate their support.

Conflicts of Interest: The authors declare no conflicts of interest.

References

1. Behe, B.; Dennis, J.; Hall, C.; Hodges, A.; Brumfield, R. Regional marketing practices in U.S. nursery production. *HortScience* **2008**, *43*, 2070–2075. [[CrossRef](#)]
2. Hall, C.; Hodges, A.; Khachatryan, H.; Palma, M. Economic contributions of the green industry in the United States in 2018. *J. Environ. Hortic.* **2020**, *38*, 73–79. [[CrossRef](#)]
3. Toscano, S.; Ferrante, A.; Romano, D. Response of Mediterranean ornamental plants to drought stress. *Horticulturae* **2019**, *5*, 6. [[CrossRef](#)]
4. Majsztrik, J.; Fernandez, R.; Fisher, P.; Hitchcock, D.; Lea-Cox, J.; Owen, J.; White, S. Water use and treatment in container-grown specialty crop production: A review. *Water Air Soil Pollut.* **2017**, *228*, 3272. [[CrossRef](#)] [[PubMed](#)]
5. Álvarez, S.; Sánchez-Blanco, M. Changes in growth rate, root morphology and water use efficiency of potted *Callistemon citrinus* plants in response to different levels of water deficit. *Sci. Hortic.* **2013**, *156*, 54–62. [[CrossRef](#)]
6. Cameron, R.W.F.; Harrison-Murray, R.S.; Scott, M.A. The use of controlled water stress to manipulate growth of container-grown *Rhododendron* cv. Hoppy. *J. Hortic. Sci. Biotechnol.* **1999**, *74*, 161–169. [[CrossRef](#)]
7. Scagel, C.F.; Bi, G.; Fuchigami, L.H.; Regan, R.P. Effects of Irrigation Frequency and Nitrogen Fertilizer Rate on Water Stress, Nitrogen Uptake, and Plant Growth of Container-grown *Rhododendron*. *HortScience* **2011**, *46*, 1598–1603. [[CrossRef](#)]
8. Freeman, D.; Gupta, S.; Smith, D.H.; Maja, J.M.; Robbins, J.; Owen, J.S., Jr.; Peña, J.M.; de Castro, A.I. Watson on the Farm: Using Cloud-Based Artificial Intelligence to Identify Early Indicators of Water Stress. *Remote Sens.* **2019**, *11*, 2645. [[CrossRef](#)]
9. de Castro, A.I.; Shi, Y.; Maja, J.M.; Peña, J.M. UAVs for Vegetation Monitoring: Overview and Recent Scientific Contributions. *Remote Sens.* **2021**, *13*, 2139. [[CrossRef](#)]
10. Matese, A.; Czarnecki, J.M.P.; Samiappan, S.; Moorhead, R. Are unmanned aerial vehicle based hyperspectral imaging and machine learning advancing crop science? *Trends Plant Sci.* **2023**, *29*, 196–209. [[CrossRef](#)]
11. Lowe, A.; Harrison, N.; French, A. Hyperspectral image analysis techniques for the detection and classification of the early onset of plant disease and stress. *Plant Methods* **2017**, *13*, 80. [[CrossRef](#)] [[PubMed](#)]
12. Behmann, J.; Acebron, K.; Emin, D.; Bennertz, S.; Matsubara, S.; Thomas, S.; Rascher, U. Specim IQ: Evaluation of a new, miniaturized handheld hyperspectral camera and its application for plant phenotyping and disease detection. *Sensors* **2018**, *18*, 441. [[CrossRef](#)]
13. Duarte-Carvajalino, J.; Silva-Arero, E.; Gómez-Vinasco, G.; Torres-Delgado, L.; Ocampo-Paez, O.; Castaño-Marín, Á. Estimation of water stress in potato plants using hyperspectral imagery and machine learning algorithms. *Horticulturae* **2021**, *7*, 176. [[CrossRef](#)]

14. Sytar, O.; Brestič, M.; Živčák, M.; Olšovská, K.; Kovár, M.; Shao, H.; He, X. Applying hyperspectral imaging to explore natural plant diversity towards improving salt stress tolerance. *Sci. Total Environ.* **2017**, *578*, 90–99. [[CrossRef](#)] [[PubMed](#)]
15. Osco, L.; Ramos, A.; Moriya, É.; Bavaresco, L.; Lima, B.; Estrabí, N.; Araújo, F. Modeling hyperspectral response of water-stress-induced lettuce plants using artificial neural networks. *Remote Sens.* **2019**, *11*, 2797. [[CrossRef](#)]
16. Susić, N.; Žibrat, U.; Širca, S.; Strajnar, P.; Razinger, J.; Knapič, M.; Stare, B. Discrimination between abiotic and biotic drought stress in tomatoes using hyperspectral imaging. *Sens. Actuators B Chem.* **2018**, *273*, 842–852. [[CrossRef](#)]
17. Nagasubramanian, K.; Jones, S.; Singh, A.; Sarkar, S.; Ganapathysubramanian, B. Plant disease identification using explainable 3D deep learning on hyperspectral images. *Plant Methods* **2019**, *15*, 98. [[CrossRef](#)] [[PubMed](#)]
18. Näsi, R.; Viljanen, N.; Kaivosoja, J.; Hakala, T.; Pandžić, M.; Markelin, L.; Honkavaara, E. Assessment of various remote sensing technologies in biomass and nitrogen content estimation using an agricultural test field. *ISPRS Arch.* **2017**, *XLII-3/W3*, 137–141. [[CrossRef](#)]
19. Virnodkar, S.; Pachghare, V.; Patil, V.; Jha, S. Remote Sensing and Machine Learning for Crop Water Stress Determination in Various Crops: A Critical Review. *Precis. Agric.* **2020**, *21*, 1121–1155. [[CrossRef](#)]
20. Wong, C.; Gilbert, M.; Pierce, M.; Parker, T.; Palkovic, A.; Gepts, P.; Buckley, T. Hyperspectral Remote Sensing for Phenotyping the Physiological Drought Response of Common and Tepary Bean. *Plant Phenomics* **2023**, *5*, 21. [[CrossRef](#)]
21. Park, S.; Ryu, D.; Fuentes, S.; Chung, H.; O’Connell, M.; Kim, J. Dependence of CWSI-Based Plant Water Stress Estimation with Diurnal Acquisition Times in a Nectarine Orchard. *Remote Sens.* **2021**, *13*, 2775. [[CrossRef](#)]
22. Liu, H.; Yu, T.; Hu, B.; Hou, X.; Zhang, Z.; Liu, X.; Bao, Q. UAV-Borne Hyperspectral Imaging Remote Sensing System Based on Acousto-Optic Tunable Filter for Water Quality Monitoring. *Remote Sens.* **2021**, *13*, 4069. [[CrossRef](#)]
23. Vairavan, C. Hyperspectral Imaging of Soil and Crop: A Review. *J. Exp. Agric. Int.* **2024**, *46*, 48–61. [[CrossRef](#)]
24. Zeng, X.; Wang, Q.; Liu, J.; Chen, Z. Hyperspectral indices optimized for real-time monitoring of water stress in maize fields. *Remote Sens.* **2022**, *14*, 2829. [[CrossRef](#)]
25. Fields, J.S.; Owen, J.S., Jr.; Scoggins, H.L. The Influence of Substrate Hydraulic Conductivity on Plant Water Status of an Ornamental Container Crop Grown in Suboptimal Substrate Water Potentials. *HortScience* **2017**, *52*, 1419–1428. [[CrossRef](#)]

Disclaimer/Publisher’s Note: The statements, opinions and data contained in all publications are solely those of the individual author(s) and contributor(s) and not of MDPI and/or the editor(s). MDPI and/or the editor(s) disclaim responsibility for any injury to people or property resulting from any ideas, methods, instructions or products referred to in the content.